The Planar Multipole Resonance Probe: A Minimally Invasive Monitoring Concept for Plasma-Assisted Dielectric Deposition Processes

Dennis Pohle, *Graduate Student Member, IEEE*, Christian Schulz, *Member, IEEE*, Moritz Oberberg, Peter Awakowicz, and Ilona Rolfes, *Member, IEEE*

***Abstract*— In this article, a novel minimally invasive approach to plasma monitoring in the challenging environment of dielectric deposition processes based on the planar multipole resonance probe (pMRP) is presented. By placing the sensor on the plasma-remote side of a dielectric substrate to be coated, perturbations of the process due to its presence can be significantly reduced. Since the electric field of the sensor is able to penetrate dielectric layers, a plasma supervision through the substrate is enabled. To investigate the effect of increasing coating thicknesses on the measurement performance for a broad spectrum of materials and plasma conditions, the results of extensive 3-D full-wave simulations performed with CST Microwave Studio are evaluated. Finally, real-time monitoring results of an argon–oxygen plasma during a sputter deposition with aluminum oxide on a polyethylene terephthalate (PET) film substrate together with a comparison to external process parameters are presented. The results demonstrate both the applicability of the proposed concept and its insensitivity to additional dielectric coatings.**

***Index Terms*— Active plasma resonance spectroscopy (APRS), dielectric deposition, planar multipole resonance probe (pMRP), plasma diagnostics, thin-film technology, 3-D electromagnetic simulations.**

I. Introduction

THIN-FILM technologies and processes are an indispensable tool for modern product development in numerous industries. The term thin-film technology encompasses various techniques for depositing a thin material layer—both dielectric and metallic—onto a substrate or onto previously deposited layers [1]. The vast amount of existing processes can be roughly divided into physical and chemical deposition techniques, which can be further subdivided into physical vapor deposition (PVD), chemical vapor deposition (CVD), and chemical solution deposition (CSD) [1], [2]. The latter utilize liquid precursor substances to achieve chemical reactions and layer growth on the substrate, whereas PVD and CVD processes are performed in the gas phase, as the names already imply. In general, both are advantageous over CSD when it comes to coating properties, such as hardness, wear resistance, temperature and stress durability, or corrosion resistance [3]. Nevertheless, CSD processes are cost effective, rather simple, and highly scalable since no complex vacuum technology is involved [2]. PVD and CVD comprise a wide range of different techniques with the same objective. However, their characteristics sometimes coalesce with each other making it difficult to distinguish between both. The main difference here is whether a chemical reaction is involved and, if so, the location of this reaction. While in case of CVD, it occurs directly at the surface boundary of the intended substrate, the layer growth in PVD can be either passive or with an optional chemical reaction in the gas phase prior to the condensation process. Usually, CVD processes are carried out at much higher temperatures compared with PVD processes [4]. Typical layer thicknesses are in the range of a few nanometers up to some micrometers [4]. Apart from PVD and CVD processes, other advanced techniques, such as molecular beam epitaxy or atomic layer deposition, even enable a reduction to single molecular or atomic layers [5], [6]. Therefore, thin-film technologies play a key role in the fabrication of semiconductor devices and synthesis of nanomaterials. For instance, a large number of technological breakthroughs in ultralarge-scale integration (ULSI) has resulted from advances in thin-film processing techniques and has enabled the development of modern ICs as well as other electronic devices, including photovoltaic cells, batteries, magnetic/optical memory, liquid crystal displays (LCDs), or advanced sensors/actuators [7]. However, the field of application is not limited to high-end devices but also includes the fabrication of functional coatings for profane low-priced daily life items, such as glasses [8] or polyethylene terephthalate (PET) bottles [9].

Manuscript received October 15, 2019; revised January 4, 2020; accepted January 7, 2020. Date of publication April 6, 2020; date of current version June 3, 2020. This article is an expanded version from the IEEE MTT-S International Microwave Workshop Series on Advanced Materials and Processes 2019 (IMWS-AMP 2019), July 16–18, 2019, Bochum, Germany. *(Corresponding author: Dennis Pohle.)*

Dennis Pohle, Christian Schulz, and Ilona Rolfes are with the Institute of Microwave Systems, Ruhr University Bochum, 44801 Bochum, Germany (e-mail: dennis.pohle@rub.de; christian.schulz-hfs@rub.de; ilona.rolfes@rub.de).

Moritz Oberberg and Peter Awakowicz are with the Institute for Electrical Engineering and Plasma Technology, Ruhr University Bochum, 44801 Bochum, Germany (e-mail: oberberg@aept.rub.de; awakowicz@aept.rub.de).

Color versions of one or more of the figures in this article are available online at http://ieeexplore.ieee.org.

Digital Object Identifier 10.1109/TMTT.2020.2974835

TABLE I
OVERVIEW OF PLASMA DIAGNOSTIC CONCEPTS REGARDING THEIR ADVANTAGES AND DISADVANTAGES IN DEPOSITION PROCESSES

Diagnostic Method / Sensor	Advantages	Disadvantages
Langmuir Probe [35], [46]	- Established, well-known diagnostic concept - Insensitive to metallic deposition - Local, direct, and time resolved information	- Sensitive to dielectric deposition due to insulation of probe tip - Perturbation of the plasma due to sensor's presence
Multipole Resonance Probe (spherical design) [46]	- Insensitive to dielectric deposition - Local, direct, and time resolved information - Easy evaluation: observation of resonance - Economical	- Sensitive to metallic deposition - Perturbation of the plasma due to sensor's presence
APRS probes based on electromagnetic approach, e.g. Curling Probe, Hairpin Probe [35]	- Relatively simple setup - Depending on design: minimally invasive	- Complex mathematical description under consideration of full Maxwell equations - Ambiguous resonance behavior - Depending on design: invasive
Optical Emission Spectroscopy [47]	- Non-invasive - Robust and precise if plasma model is available - Identification of chemical species	- Useful correlations of emission spectra to plasma conditions are difficult to obtain - Complex model of specific plasma required - Difficult interpretation of ambiguous results - Deposited material on the observation window can significantly affect the measured signal, e.g. selective absorption of emission

Low-pressure plasmas play a key role in many of the existing PVD/CVD processes, e.g., in sputter deposition and its variations, such as ion beam sputtering or plasma ion-assisted deposition, as well as in plasma-enhanced and plasma-activated CVD. Plasma-assisted thin-film processes are widely used for the production of energy-efficient, optical, electrically operating, protective, decorative, or multifunctional coatings with versatile characteristics [9]–[11]. Here, plasmas are required as a source of high-energy ions, as highly chemically active zones, for surface activation, etching, and pre-cleaning/sterilization. As an example, in sputter deposition, atoms or molecules are released from a solid target material due to the steady ion bombardment inside the plasma. Subsequently, the evaporated target particles are accelerated toward the intended substrate by applying an electric field. Due to condensation as a result of the impact, the desired layer is formed. Depending on the applied process gas as well as other (optional) reactive gas additives, target particles can be subject to chemical reactions prior to colliding with the substrate. This so-called reactive sputtering allows to create layers of material compounds on the substrate, which differ from the initial target material [12].

A stable and well-defined plasma state is a crucial aspect for the whole deposition process [13]–[16]. To ensure a high quality as well as a batch-to-batch consistency of the coatings, important parameters of the plasma, such as electron density n_e, collision frequency ν, and electron temperature T_e, are of particular interest for process control. For this purpose, a suitable sensor system and measurement concept is required. In particular, regarding automated industrial-scale production, a precise long-term as well as real-time monitoring is essential, in order to detect unwanted process fluctuations, which otherwise might have a severe impact on yield and costs [17], [18].

Although several plasma diagnostic concepts exist, the vast majority of the plasma industry still relies on external parameters, such as generator power, gas fluxes, and pressure, to control the production process [19]. This can be explained by the fact that either process-related and/or economic considerations might disqualify the respective diagnostic option.

However, external parameters only provide indirect information about the actual plasma condition and may not be directly correlated with thin-film properties or etching results [20]. Yet, the rising demands of modern coating processes and applications lead to an ever-increasing complexity of the plasma phenomena that must be considered. Table I summarizes the advantages and disadvantages of the existing diagnostic options in the context of deposition processes. Due to the lack of simultaneously precise, fast, economical, unambiguous, deposition-insensitive, and minimally invasive concepts, which are easy to evaluate, a targeted control of the plasma processes is thus hardly possible. Hence, there is a strong demand for industry compatible approaches.

A promising candidate for supervision of plasma-assisted dielectric deposition processes was first introduced in [21] and discussed in detail in [22]: the so-called planar multipole resonance probe (pMRP). Derived from the standard spherical multipole resonance probe (MRP) [23], the compact plasma sensor can be flush-mounted in the chamber wall of a plasma reactor allowing for a minimally invasive process monitoring. Based on active plasma resonance spectroscopy (APRS), the pMRP represents a stationary and industry compatible plasma measurement concept. In [22], a prototype was tested in a double inductively coupled argon plasma as a proof-of-concept study. Further design improvements, including significantly increased high-temperature resistance, were presented in [24] and [25]. Moreover, recent advances in the mathematical description of the sensor [26]

enable—in contrast to an arbitrary resonant structure—a correlation of the observed resonances to the prevailing electron density in a quantitative manner.

In light of the previous studies, further scientific research concerning the applicability of the pMRP for long-term monitoring within the challenging environment of deposition processes is of particular interest for thin-film processing. In [27], we already presented first results with the pMRP, which were obtained during measurements within a dielectric sputter deposition process. Instead of mounting the sensor within the reactor wall, the concept of placing it directly on the plasma-remote side of a dielectric substrate to be coated was first introduced. In this article, we further expand upon that concept and discuss its performance and limitations in greater detail. In particular, we also consider the influence of the collision frequency and different materials. Starting in Section II with plasma fundamentals and theoretical considerations based on the recently published model [26], the novel concept is described in detail in Section III. Section IV presents the results of extensive 3-D electromagnetic simulations of the system consisting of probe, plasma, substrate, and coating covering a variety of plasma conditions, materials, and coating thicknesses. Finally, measurement results of a long-term real-time plasma monitoring obtained within a dielectric sputter deposition process together with a direct side-by-side comparison of the supervised external process parameters are shown in Section V. Section VI concludes this article.

II. Fundamentals

A. Plasma

Low-pressure plasmas used in thin-film processing, for instance, are (partly) ionized gases, which are excited and sustained by an external energy source, e.g., an inductive, capacitive or microwave feeding [28]. The fundamental plasma stimulus as a consequence of the energy injection in free electrons in a neutral gas is mainly driven by collisions between high-energetic electrons with other neutral gas constituents. If the electron energy is above a certain threshold, they are able to ionize the gas atoms. Thus, additional electrons are accelerated, which can collide with further particles. In case an excited atom returns to a lower energy state, light of a characteristic wavelength is emitted. Depending on the applied gas type(s) and the occurring chemical reactions, this can cause the typical glowing and color of a plasma, if the wavelength is in the visible spectrum, e.g., purple for pure argon [29]. Due to the free electrons and ions, the resulting plasma is electrically conductive, showing a quasi-neutrality from the outside, which is in a dynamic equilibrium [30]. Yet, without a steady energy injection, matter would return to its neutral state as a result of electron–ion recombination. The charged particles in the plasma try to follow the external electric field of the used excitation source. Thus, fluctuations of the respective local density occur and an electric field arises between oppositely charged regions, which is proportional to their separation length. The occurring Coulomb force attempts to restore the equilibrium resulting in a harmonic oscillation of the density due to the inertia of the particles. These eigenfrequencies are referred to as natural plasma electron frequency ω_{pe} and natural plasma ion frequency ω_{pi} [30]

$$\omega_{\mathrm{pe}} = \sqrt{\frac{e^2\ n_{\mathrm{e}}}{\varepsilon_0\ m_{\mathrm{e}}}} \tag{1}$$

$$\omega_{\mathrm{pi}} = \sqrt{\frac{e^2\ n_{\mathrm{i}}}{\varepsilon_0\ m_{\mathrm{i}}}} \tag{2}$$

with elementary charge e, electron density n_{e}, ion density n_{i}, vacuum permittivity ε_0, electron mass m_{e}, and ion mass m_{i}.

The respective particles are just able to follow the source's electric field as long as the frequency of this field stays below ω_{pe} and ω_{pi}. Since m_{i} is significantly larger than m_{e}, ω_{pi} is considerably lower than ω_{pe}. In RF excited processes, e.g., inductive or capacitive, the excitation frequencies are usually far above ω_{pi} but lower than ω_{pe}. Therefore, the ions remain at rest, while the excitation energies can be absorbed by the electrons.

One important parameter for deposition processes is the electron density n_{e}, which is directly linked to ω_{pe} by (1). The electron collision frequency ν is another crucial factor for process control. As mentioned earlier, collisions between the particles are fundamental processes within the plasma. The parameter ν denotes the attenuation of the plasma oscillation and thus considers losses inside the plasma. In general, it is given by [31]

$$\nu = \frac{p_{\mathrm{gas}}}{k_{\mathrm{B}} T_{\mathrm{gas}}} \cdot K(T_e) \tag{3}$$

with gas pressure p_{gas}, Boltzmann's constant k_{B}, gas temperature T_{gas}, and rate constant $K(T_{\mathrm{e}})$ depending on the electron temperature T_{e} as well as the applied process gas. Equation (3) might be further modified by considering an additional kinetic collision process denoting deflections of electrons caused by the electromagnetic field of an inserted probe as shown in [32] and [33] for the spherical MRP, for instance.

In addition, due to the steady bombardment with electrons, surfaces being in contact with the plasma become negatively charged. Hence, a so-called plasma sheath is formed around these surfaces, e.g., around the reactor walls or an *in situ* probe, as an electron depletion zone mainly consisting of vacuum and a small amount of ions. According to [32], the thickness of the plasma sheath can be assumed by $\delta = 3 \cdot \lambda_{\mathrm{Debye}}$, where λ_{Debye} is the so-called Debye length describing the distance within which the potential of a point charge has decreased to $1/e$. The Debye length itself is given by [30]

$$\lambda_{\mathrm{Debye}} = \sqrt{\frac{\epsilon_0\ k_{\mathrm{B}} T_{\mathrm{e}}}{n_{\mathrm{e}} e^2}}. \tag{4}$$

Consequently, the plasma sheath thickness is interdependent with the plasma parameters n_{e} and T_{e}.

B. Ideal Planar Multipole Resonance Probe

The outcome of the plasma process strongly depends on its internal parameters, which are interrelated in a complex way with the external ones, such as excitation power, gas

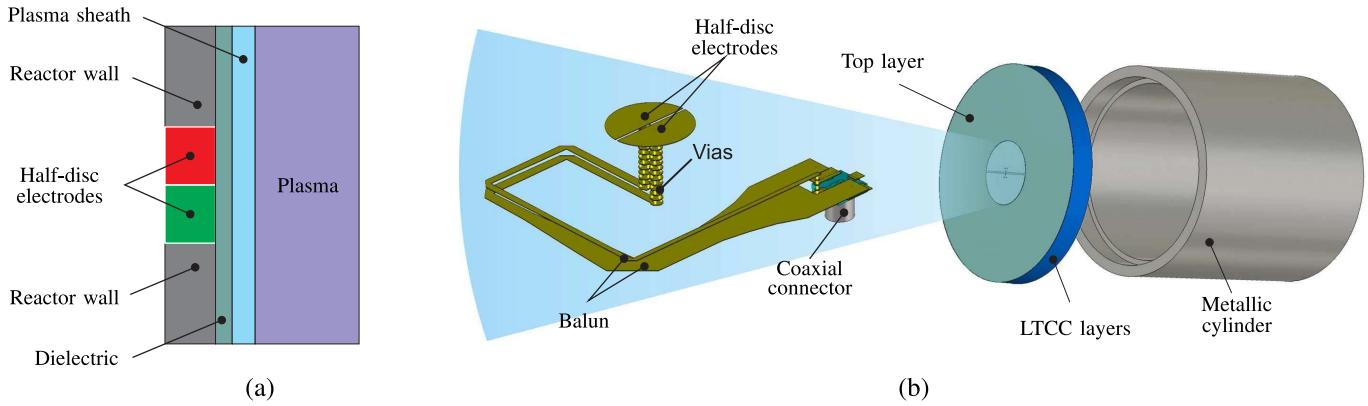

Fig. 1. pMRP. (a) Ideal model according to [26] . (b) Developed sensor design with stacked components [24], [25].

pressure, and gas flow rate. Therefore, a direct supervision of the internal plasma state together with a feedback control of the process is crucial for yield and quality improvements. A suitable and well-known *in situ* approach is the so-called APRS. APRS is based on the universal characteristic of all low-pressure plasmas to resonate near the plasma electron frequency when excited with a high-frequency signal [34]. Various implementations of this basic principle have recently been proposed. An overview can be found in [35], for instance. The concept can be further classified into electromagnetic and electrostatic methods [36]. The former is based on the excitation of standing waves in the plasma reactor volume. The occurring cavity resonances are already present in vacuum and are just further affected by the plasma presence. The proportionality between the resonance and plasma electron frequencies can be used for the determination of the electron density. However, in order to describe the interrelations, a complex mathematical description under consideration of the full Maxwell equations is necessary. On the other hand, electrostatic methods work below the plasma electron frequency. Thus, the resonance excitation is based on a different mechanism. In contrast to electromagnetic methods, there is no radiation of waves into the reactor. Instead, only surface waves are excited at the boundary between the dielectric surrounding the *in situ* probe and the plasma leading to a localized penetration of the fields into the reactor volume. Hence, an electrostatic approximation is sufficient to adequately characterize the physical interactions. The resulting resonance behavior of the system consisting of probe and plasma can be described using an equivalent resonance circuit model. A general description for an arbitrarily shaped N-electrode probe was presented in [36]. The MRP represents the optimized approach of this general concept [23]. Consisting of two symmetrically powered metallic hemispheres, which are separated by an infinitesimal small gap and inserted into a dielectric sphere, the design allows for a significant simplification of the mathematical formalism and a derivation of an analytical solution for the complex admittance $\underline{Y}$ of the equivalent resonance circuit. This admittance can be used to determine the desired plasma parameters n_e, ν, and T_e. The ideal MRP concept was transferred to different real prototype designs, which were validated in several studies [32], [37], [38]. However, the insertion of the MRP into the reactor volume and the associated disruption of the plasma might be problematic for certain processes and applications. Hence, a minimally invasive sensor design derived from the MRP, the so-called pMRP, was first introduced in [21] and further investigated in [22]. The model of the ideal pMRP consists of two planar metallic half-disc electrodes that are separated by an infinitesimal insulation and covered with an additional dielectric layer. At the boundary between dielectric and plasma, a plasma sheath arises. Fig. 1(a) shows the ideal model according to [26] with the probe head placed within the reactor wall. An insulation assumed infinitesimal separates the electrodes and reactor wall. Analogous to the standard MRP, an analytical solution for the probe-plasma system's admittance could be recently derived for the ideal pMRP [26]

$$\underline{Y} = \sum_{n=1}^{\infty}\sum_{\tilde{m}=0}^{\infty} A_{2\tilde{m}+1,n}\frac{4\pi\epsilon_0\omega_{\mathrm{pe}}^2\ R_\infty i\omega\beta_{n,2\tilde{m}+1}^{(1)^2}}{2\omega_{\mathrm{pe}}^2\eta_{n,2\tilde{m}+1}^2 - i\omega\nu - 2\omega^2} \tag{5}$$

with

$$A_{2\tilde{m}+1,n} = (j_{2\tilde{m}+1,n})J_{2(\tilde{m}+1)}^2(j_{2\tilde{m}+1,n})e^{-2k_{n,2\tilde{m}+1}(d+\delta)} \tag{6}$$

and

$$\eta_{n,2\tilde{m}+1} = \frac{1}{\sqrt{2}}\sqrt{1-\left(1-\frac{2}{\varepsilon_{\mathrm{r,D}}\cosh\left(k_{n,2\tilde{m}+1}d\right)+1}\right)e^{-2\delta k_{n,2\tilde{m}+1}}} \tag{7}$$

and

$$k_{n,2\tilde{m}+1} = j_{2\tilde{m}+1,n}R_\infty^{-1} \tag{8}$$

where $\varepsilon_{\mathrm{r,D}}$ is the permittivity, d is the thickness of the dielectric covering the electrodes, δ is the thickness of the plasma sheath, $j_{2\tilde{m}+1,n}$ is the nth root of the $(2\tilde{m}+1)$th Bessel function, $J_{2(\tilde{m}+1)}$ is the Bessel function of order $2(\tilde{m}+1)$, $\beta_{n,2\tilde{m}+1}^{(1)}$ includes the geometric parameters of the probe, and R_∞ is the radius of the boundary surface, which is assumed as infinite in the model. $\tilde{m}$ denotes the fact that only odd values $m = 2\tilde{m}+1$ contribute for the calculation since the admittance vanishes for even m. Further investigations showed that a sufficient convergence behavior of (5) can be

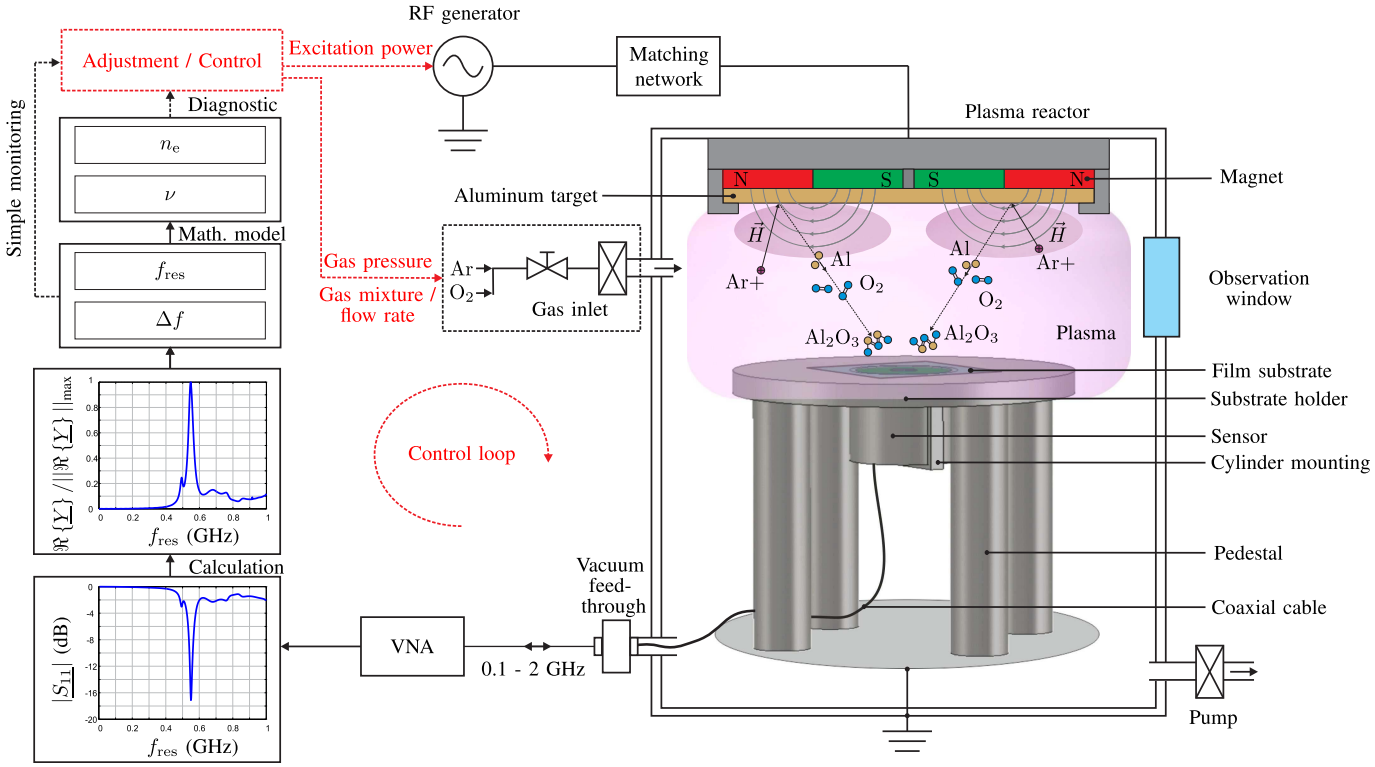

Fig. 2. Proposed minimally invasive monitoring concept for plasma-assisted dielectric depositions on dielectric film substrates. Subsequent feedback loop for process control on the basis of the evaluated plasma parameters. As example, deposition of aluminum oxide in a magnetron CCP reactor using an argon–oxygen plasma.

obtained by limiting the upper boundaries in the double series to $N_{\max} = 125$ and $\tilde{M}_{\max} = 1$ as well as the boundary surface radius to $R_\infty = 40\ \mathrm{R_S}$, where $\mathrm{R_S}$ is the electrode radius [26]. The converged spectra of $\underline{Y}$ show one dominant resonance peak from which the resonance frequency can be extracted

$$\omega_{\mathrm{res}} \propto \omega_{\mathrm{pe}} \propto \sqrt{n_{\mathrm{e}}}. \tag{9}$$

As can be seen, a rising ω_{pe} results in a rising ω_{res}. The explicit proportionality can be derived for a specific probe design using the converged spectrum of $\underline{Y}$, as shown in [26]. Therefore, together with (1), the electron density n_{e} can be estimated from the resonance frequency.

Moreover, since the collision frequency ν is interrelated with losses inside the plasma, it is linked to the width $\Delta\omega$ of the observed resonance

$$\nu \propto \Delta\omega = \mathrm{FWHM}\left\{\frac{\Re\{\underline{Y}\}}{||\Re\{\underline{Y}\}||_{\max}}\right\} \tag{10}$$

where FWHM is the full width at half maximum of the normalized real part of the admittance $\underline{Y}$. Here, a rising ν leads to a rising $\Delta\omega$.

III. Sensor Design and Measurement Concept

Fig. 1(b) shows the developed sensor prototype based on the ideal pMRP, which is used in this article. Its specific design was first introduced in [24] and discussed in more detail in [25]. As a substrate material, low-temperature co-fired ceramics (LTCCs) have been chosen due to their high-temperature resistance and good RF properties. All required sensor components are vertically stacked within the circularly shaped LTCC layers and connected with vias. Henceforth, the name of this specific design is referred to as stacked pMRP (spMRP). As in the ideal pMRP model, the sensor consists of a planar probe head realized as two half-disk electrodes. Unlike the infinitely small separation of the ideal model, a minimal separation distance of 200 µm could be fabricated. Due to the matching of the probe, a specific half-disk radius is only able to cover a limited frequency range and thus needs to be optimized for a specific electron density range. In this article, a prototype with a radius of 5 mm is chosen. In order to achieve the required balanced feeding of the electrodes, a tapered microstrip balun is integrated into the design in the subjacent LTCC layers, which can be fed using a back-mounted coaxial connector. To minimize the mutual coupling with the probe head, the balun is bended around the probe center and is further separated with layers in between. An additional dielectric top layer covers the electrodes to achieve a separation to the surrounding plasma. The ratio between the thickness of this separation and that of the deposited dielectric layers has an impact on the sensor's sensitivity to the coating [22], [39]. In this article, a prototype with a DuPont951PT ceramic layer having a fired thickness of around 100 µm is used. Since this is 2.5 times thicker than the glass top layer of the prototype used in [27], an increased insensitivity is expected in comparison. In contrast to the ideal model, the insulation distance between reactor wall and electrodes is not infinitely small. Since a metallic layer directly adjacent to the probe head leads to matching problems and

additional cavity resonances in practice, which significantly degrade the measurement performance of the sensor, the distance was set to 12 mm. However, recent results already showed that the ideal model can be adapted to account for this difference in geometry [40].

Furthermore, the spMRP is placed inside a metallic cylinder to guarantee a flush-mounted installation within the substrate holder of the proposed measurement setup, as shown in Fig. 2. Here, the cylinder is attached right behind a film substrate to be coated. Therefore, the probe head is located on its plasma-remote side, thus resulting in a minimized influence on the plasma itself. Since the substrate per se remains unchanged during the process, it can be seen as part of the sensor and considered in the model, e.g., via the resulting effective permittivity.

In the described scenario, a so-called capacitively coupled plasma (CCP) reactor in magnetron arrangement is depicted. Its basic setup consists of a driven electrode and a grounded one (here, the substrate holder) placed on opposite sites. In this article, an RF excitation at 13.56 MHz is applied. Other excitations, e.g., dc, or different reactor types are also possible. The specific reactor used in this article is discussed in greater detail in [41]. The target (here, aluminum) is attached below the driven electrode, while the film substrate is placed on the grounded one. The plasma is generated mainly between the electrodes. A controllable gas inlet supplies the preevacuated reactor chamber with the necessary process gases. Additional magnets above the target increase the electron energy in their close proximity and lead to an increased ionization rate. Consequently, a higher electron density at the target is achieved, thus resulting in a higher sputter rate. During the process, the desired material compound (here, Al_2O_3) condenses on the film substrate. With ongoing process time, its layer thickness increases continuously. As long as dielectric material is deposited, the electric field of the sensor is able to penetrate substrate, deposited layers, and the sheath and couples into the plasma. To monitor the plasma condition, the sensor is connected with a vector network analyzer (VNA) using a vacuum feedthrough for the coaxial cable. Subsequently, the complex reflection coefficient $\underline{S}_{11}$ can be evaluated and transformed toward the probe head to exclude the feeding, and the required complex admittance can be calculated by the following relation:

$$\underline{Y} = \frac{1}{Z_0} \cdot \frac{1 - \underline{S}_{11}}{1 + \underline{S}_{11}} \tag{11}$$

with $Z_0 = 50\ \Omega$ as reference impedance. The transformation can be achieved using a real one port calibration with appropriate calibration standards for highest precision, as presented in [42]. However, an adequate precision, which is sufficient in practice, is already achieved using a simple vacuum compensation by subtracting a measurement of the empty reactor from the subsequent plasma measurements, as shown in [43].

Afterward, the normalized real part of $\underline{Y}$ can be used to determine the resonance parameters $f_{\mathrm{res}} = \omega_{\mathrm{res}}/(2\pi)$ and $\Delta f = \Delta\omega/(2\pi)$, which already can be used for monitoring general fluctuations. Apart from this simple monitoring option, the measurement concept has the benefit of a real plasma diagnostic based on the ideal pMRP model, enabling the estimation of the actual prevailing electron density at the substrate location.

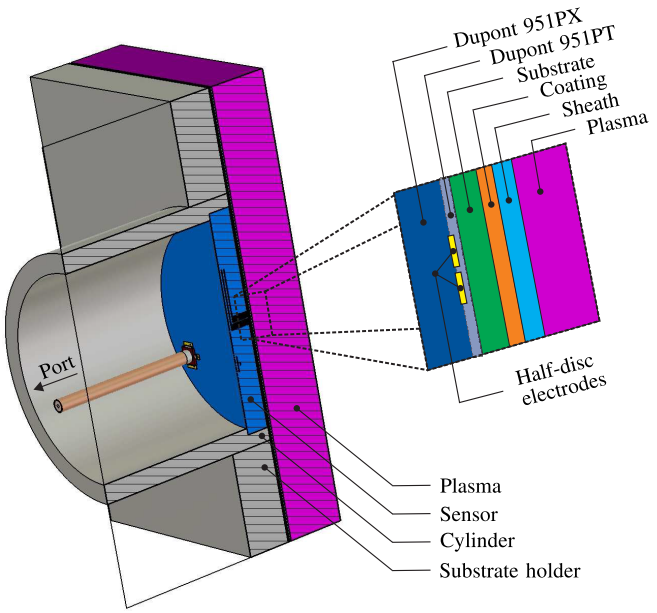

Fig. 3. Simulation model in CST Microwave Studio (cutting plane): spMRP inserted through the substrate holder/grounded reactor electrode on the substrate's plasma-remote side together with an enlarged view of the material stack [27].

IV. Simulations

To investigate the performance and limitations of the proposed concept, extensive 3-D electromagnetic full-wave simulations are performed in CST Microwave Studio covering a variety of plasma conditions, materials, and coating thicknesses. Fig. 3 shows the built-up CAD model, which is used for all subsequent simulations. Here, the complete spMRP placed inside the metallic cylinder and mounted in the substrate holder (compare Figs. 1(b) and 2) as well as the substrate to be coated, the coating layer, sheath, and the plasma are considered. As a substrate material, a PET layer with a thickness of 100 µm is chosen. The material properties and the thickness of the coating layer are varied in the following investigations, thus resulting in several pseudo-depositions processes. As mentioned earlier, a plasma sheath arises at the boundary between the coating layer and the plasma, which is modeled in the simulations as vacuum. In general, its thickness can be assumed as three Debye lengths [see (4)]. To define a reasonable thickness for the simulations, possible ranges for n_{e} and T_{e} need to be estimated in advance. According to [43], T_{e} can be assumed to be between 1 and 10 eV in low-pressure plasmas. In case of our experiments, the lower end of this range can be expected. The electron density can be assumed to be between 10^{15} and 10^{17} m^{-3} at our measurement location. Thus, considering $T_{\mathrm{e}} = 2, \ldots, 3$ eV and a medium $n_{\mathrm{e}} = 10^{16}$ m^{-3}, a thickness of 300 µm is chosen as reasonable hypothesis. This value was also used in [22] and [26] for the respective investigations. The plasma itself is

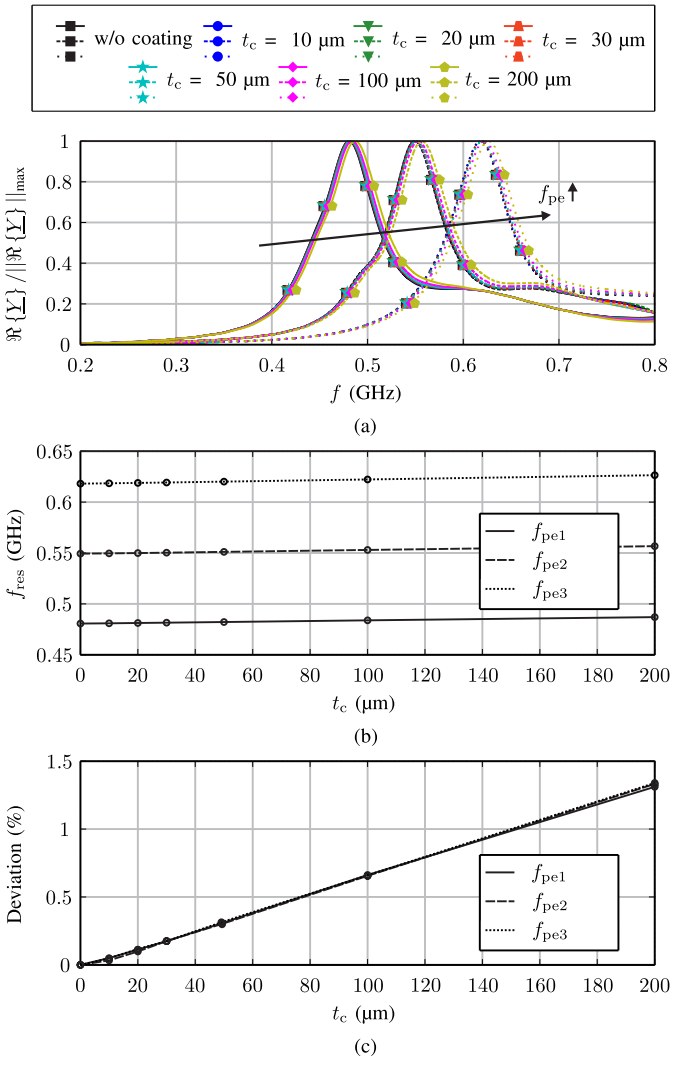

Fig. 4. (a) Simulated resonance behavior of the spMRP for a constant collision frequency $\nu = 300$ MHz and constant plasma sheath thickness $\delta = 300$ µm for three different plasma electron frequencies $f_{pe1} = 1.4$ GHz (solid lines), $f_{pe2} = 1.6$ GHz (dashed lines), and $f_{pe3} = 1.8$ GHz (dotted lines) with rising Al_2O_3 coating thickness t_c on a PET film substrate. (b) Evaluated resonance frequencies f_{res} with rising coating thickness. (c) Calculated deviation in percent with respect to the case without coating.

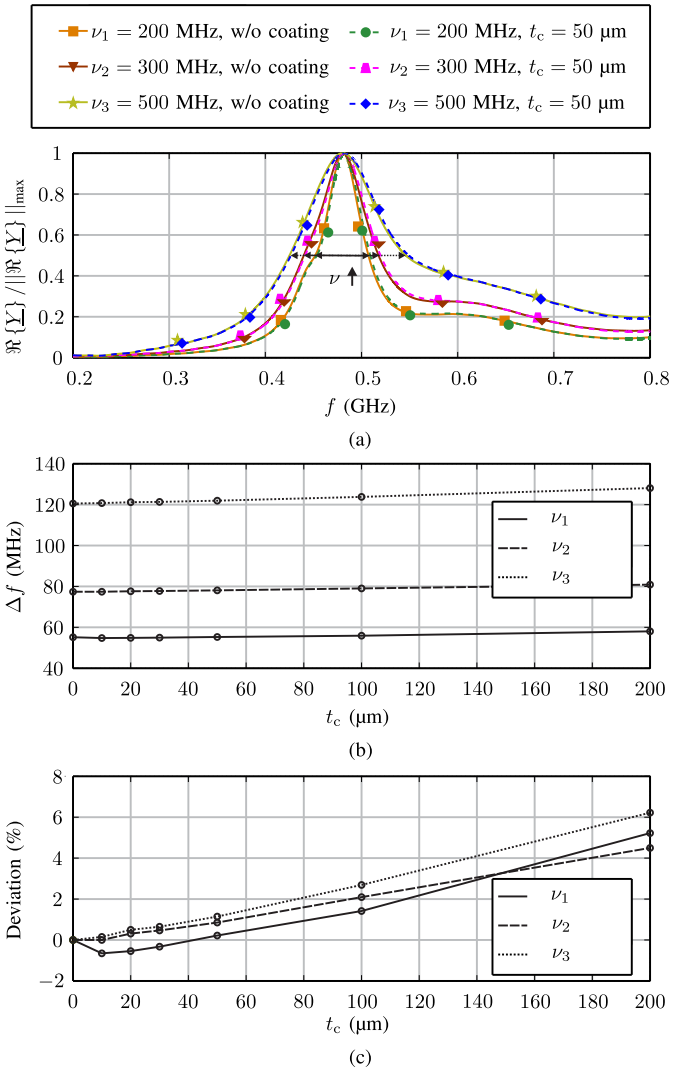

Fig. 5. (a) Simulated resonance behavior of the spMRP for a constant plasma electron frequency $f_{pe} = 1.4$ GHz and constant plasma sheath thickness $\delta = 300$ µm for three different collision frequencies $\nu_1 = 200$ MHz, $\nu_2 = 300$ MHz, and $\nu_3 = 500$ MHz with rising Al_2O_3 coating thickness t_c on a PET film substrate. (b) Evaluated resonance widths Δf with rising coating thickness. (c) Calculated deviation in percent with respect to the case without coating.

modeled as a frequency-dependent dielectric material in cold-plasma approximation according to the so-called Drude model, which is a valid assumption for low-pressure plasmas used in coating processes [37]. Within the Drude model, the dielectric properties of the plasma surrogate material are defined using ω_{pe} and ν

$$\varepsilon_{r,P}(\omega) = \varepsilon'_{r,P}(\omega) - j\varepsilon''_{r,P}(\omega) = 1 - \frac{\omega_{pe}^2}{\omega(\omega - j\nu)}. \quad (12)$$

As shown in detail in [37], a change in ω_{pe} results in a change in $\varepsilon'_{r,P}$ and $\varepsilon''_{r,P}$, whereas a change in ν only affects $\varepsilon''_{r,P}$. Consequently, for a rising ω_{pe} corresponding to an increasing n_e, the resonance frequency increases accordingly, whereas a rising ν causes broadening of the resonance width. As described in Section II-B, the electromagnetic field of the spMRP has only a restricted penetration depth into the plasma (see also [24], [25]). Therefore, the simulated plasma volume can be limited to 70 mm × 70 mm × 10 mm instead of modeling the complete reactor. For all simulations performed in this article, a frequency-domain solver with a tetrahedral mesh is used. The frequency-domain solver is advantageous for the simulation of resonant structures, while the tetrahedral mesh is well suited to discretize the cylindrical structures of the probe. The global mesh definition is given by "cells per wavelength" set to 4 for model as well as background and "cells per max model box edge" set to 20 for model and 1 for background. Considering the various thin layers in the model, the mesh is locally refined, in order to properly account for these critical structures and to increase the accuracy of the simulations. Here, the "maximum mesh step width" is set to 0.7, thus resulting in a tetrahedron size in the lower micrometer range. Overall, the simulations are performed with

TABLE II
OVERVIEW OF SOME TYPICAL MATERIALS USED IN INDUSTRIAL DEPOSITION PROCESSES [44], [45]

Material	Relative permittivity $\varepsilon'_{\mathrm{r,c}}$
SiO_2	3.9
Si_3N_4	7
Al_2O_3	9
Y_2O_3	15
Ta_2O_5	22
HfO_2	25
Pr_2O_3	30
TiO_2	80

TABLE III
OVERVIEW OF APPLIED MATERIALS FOR PSEUDO-DEPOSITION PROCESSES IN CST MICROWAVE STUDIO ANALOGOUS TO [44]; ALL VALUES WITH RESPECT TO 1 GHz

Material #	Relative permittivity $\varepsilon'_{\mathrm{r,c}}$	Loss tangent $\tan\delta_{\mathrm{c}}$
1	2	0.001
2	2	0.1
3	4	0.001
4	4	0.1
5	8	0.001
6	8	0.1
7	16	0.001
8	16	0.1
9	32	0.001
10	32	0.1

an average amount of around 540 000 tetrahedrons. The final mesh definition, however, is always a tradeoff between accuracy and simulation time. Yet, a further increase in the mesh density, in particular in the critical regions, did not lead to a significant change in the simulation results. Moreover, electric boundaries ($E_{\tan} = 0$) are chosen to limit the simulation domain. In addition, all simulations are performed in a fixed frequency range from 0.2 to 0.8 GHz, which is sufficient to investigate the occurring effects. A coaxial waveguide port with a line impedance of 50 Ω is used as feeding.

Fig. 4 shows the simulation results for pseudo-depositions with aluminum oxide [99.5%, $\varepsilon'_{\mathrm{r,c}} = 9.9$, and $\tan\delta = 0.0001$(at 1 MHz)] on the PET film substrate for three different plasma electron frequencies $f_{\mathrm{pe}} = \omega_{\mathrm{pe}}/(2\pi)$ at a constant collision frequency $\nu = 300$ MHz. Here, the coating thickness varies between 10 and 200 µm for each f_{pe} and, also, the case without any coating is considered. Here, a coating thickness exceeding 100 µm corresponds already to several hundred deposition cycles [44]. In Fig. 4(a), the resulting normalized real part of the admittance is depicted. As can be seen, one dominant resonance peak appears in each case, which shifts toward a higher frequency for an increasing f_{pe} value. Moreover, the resonance position and shape basically remains unchanged for all considered coating thicknesses at constant f_{pe}. Fig. 4(b) shows the evaluated resonance frequencies f_{res} over coating thickness t_c for each case. It is evident that only minor absolute changes in f_{res} with the increase in t_{c} occur, even for large thicknesses. Fig. 4(c) shows the deviation in percent with respect to the case without coating, which is below 1.5 % for $t_c = 200$ µm and is basically negligible here.

In the case of the simulation results shown in Fig. 5, f_{pe} is set constant to 1.4 GHz and ν is varied. Fig. 5(a) shows again the occurring resonance behavior. Here, the results for the case without coating and with $t_c = 50$ µm are compared as an example. It can be seen that the resonance broadens with the increase in ν. Again, resonance position and shape are practically preserved for the higher coating thickness. Fig. 5(b) shows the evaluated absolute values of the resonance width Δf over t_c for all considered cases. As for f_{res}, only a small shift can be observed. Yet, it is recognizable that thicker coatings have a higher influence on Δf than on f_{res}. Fig. 5(c) shows this fact more clearly, as it reveals a deviation of up to 6% for $t_c = 200$ µm. The reason is that losses are within the Al_2O_3 coating. A larger layer thickness provides a longer distance at which the field of the sensor is attenuated by the lossy material, resulting in an additional broadening of the resonance due to the reduced quality factor of the underlying resonance circuit. For typical coating thicknesses, however, the deviation is below 2% and can therefore be neglected in practice. Due to the vast amount of possible material compounds that can be used in industrial deposition processes, a more comprehensive investigation is needed. Table II shows the relative permittivities of some typical materials applied in deposition processes according to [44] and [45]. In order to quantify the effects on the resonance parameters f_{res} and Δf for a broad spectrum of different material properties, the presented pseudo-depositions have been extended by the materials listed in Table III. Here, rising permittivities $\varepsilon'_{\mathrm{r,c}}$ and two different loss tangents $\tan\delta_c$ regarding moderate as well as high losses have been considered. The simulations presented in the following have been performed at a constant $f_{\mathrm{pe}} = 1.4$ GHz and constant collision frequency $\nu = 300$ MHz. Fig. 6 shows the evaluated resonance parameters for the ten materials according to Table III and increasing coating thicknesses. In order to obtain these results, a total of 60 additional simulations with the complete setup according to Fig. 3 have been carried out in CST Microwave Studio.

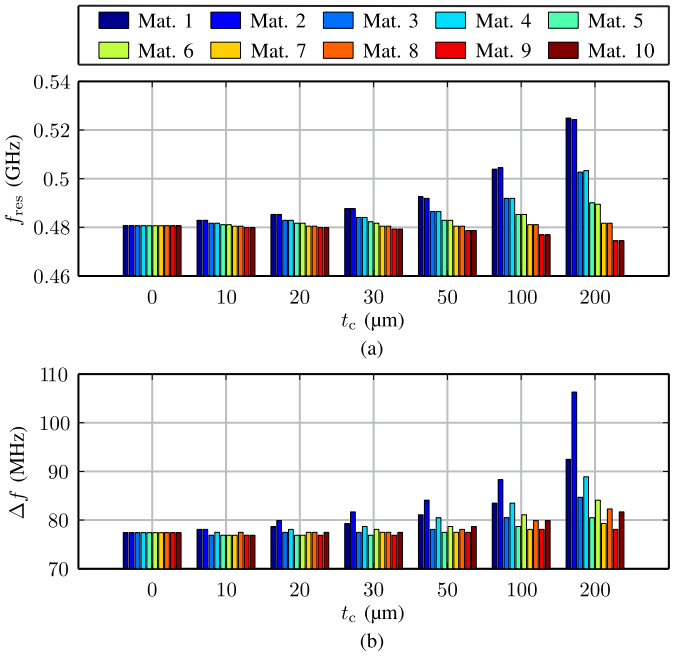

Fig. 6. Pseudo-deposition processes in CST Microwave Studio at a constant plasma electron frequency $f_{pe} = 1.4$ GHz and a collision frequency $\nu = 300$ MHz with the materials according to Table III and rising coating thicknesses t_c: (a) Evaluated resonance frequencies f_{res}. (b) Determined resonance widths Δf.

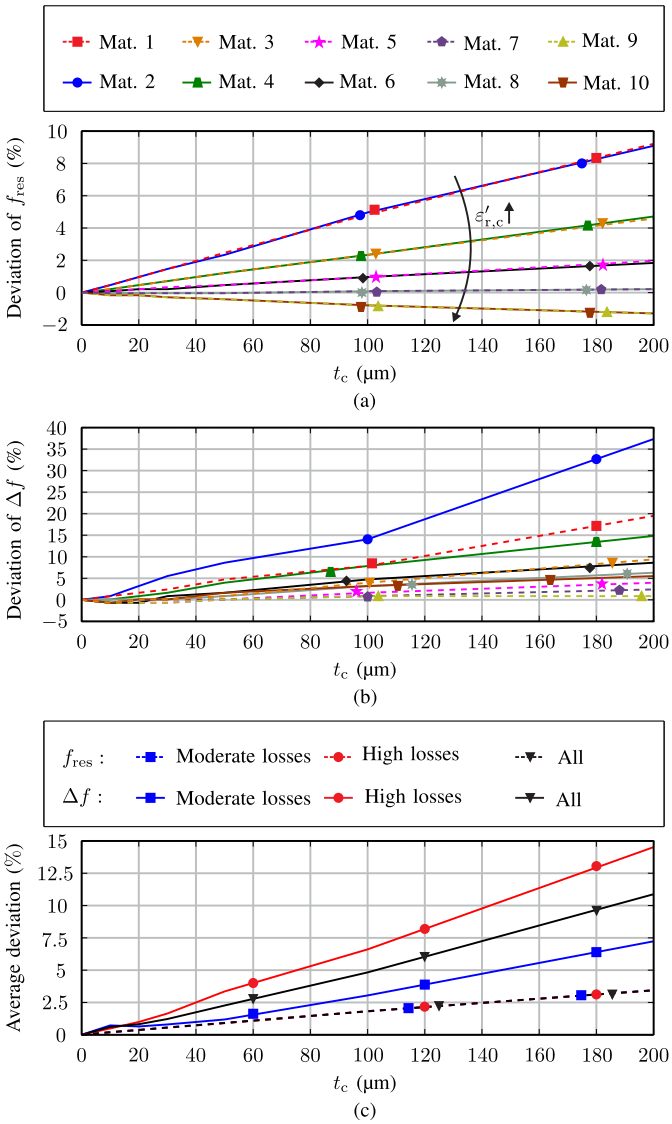

Fig. 7. Evaluation of the pseudo-deposition processes according to Table III and Fig. 6 for rising coating thicknesses. Deviation of (a) f_{res} and (b) Δf in percent with respect to the coating-free case. (c) Average deviation over all ten materials for f_{res} and Δf together with a breakdown between moderate-loss (1, 3, 5, 7, and 9) and high-loss (2, 4, 6, 8, and 10) materials.

Analogous to the previous simulations, a dominant resonance peak can be observed for all considered materials, which can be used without restrictions for the parameter extraction. Fig. 6(a) and (b) shows the evaluated resonance frequencies f_{res} and resonance widths Δf, respectively. In addition, Fig. 7(a) and (b) shows the respective deviations in percent with regard to the case without coating for all ten materials. Moreover, Fig. 7(c) shows the average deviations determined for both parameters over all materials, including a supplementary breakdown between moderate- and high-loss materials.

First of all, it is evident that the gradient of the curves in Fig. 7(a) decreases with the increase in $\varepsilon'_{r,c}$ and even becomes negative for the highest considered permittivity. In the case of materials 5–10, the maximum shift of f_{res} is below 2% for all considered thicknesses and below 1% for thicknesses up to 100 µm. In the case of materials 1–4, the maximum detected resonance shift is below 2.5% for coating thicknesses up to 50 µm. For low $\varepsilon'_{r,c}$ and very high t_c, however, the maximum deviation exceeds 9% in the worst case. The average deviation over all materials is not exceeding 3.5 % for $t_c = 200$ µm. It can be further seen that material losses have no impact on f_{res} since the related curves in Fig. 7(a) and (c) are basically identical. In the case of the resonance widths Δf, it can be observed that the deviation is below 8% for moderate losses (odd material numbers) considering coating thicknesses up to 100 µm. Yet, for the lowest $\varepsilon'_{r,c}$ and $t_c = 200$ µm, the deviation exceeds 19%. In the case of higher relative permittivities, however, the deviation is below 10% for all considered cases. In the case of high losses (even material numbers), the deviation is below 15% for thicknesses up to 100 µm. Yet, for the lowest $\varepsilon'_{r,c}$ and highest t_c, the deviation exceeds significantly 35%. Regarding higher relative permittivities, however, the deviation is below 15% for all considered cases and below 8% for thicknesses up to 100 µm. The breakdown in Fig. 7(c) highlights the differences between both loss types and reveals that the average deviation for high-loss materials is basically twice as high as for moderate-loss materials regarding coating thicknesses from 20 µm on.

As a conclusion to this section, it can be stated that coating materials with lower relative permittivities have a higher impact on both f_{res} and Δf. On the other hand, high material losses lead to an increased deviation of Δf compared to materials with lower losses. For a notable deviation in these cases, however, the coating thickness needs to be exceptionally high, which is usually not the case in typical applications. In addition, if deposition rate and material properties are

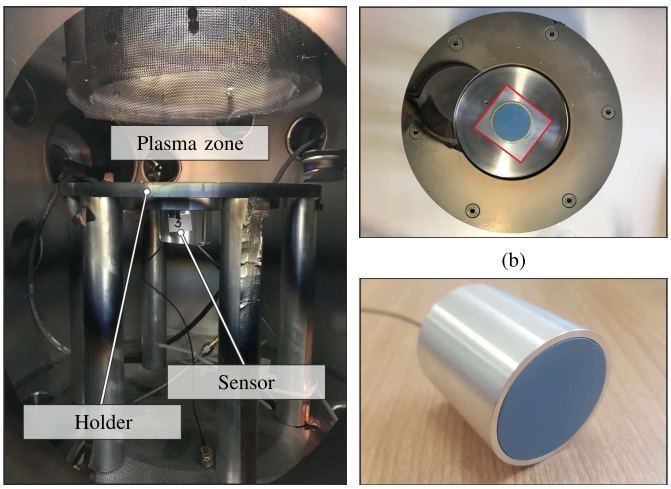

Fig. 8. Photographs of the measurement setup. (a) Inside view of the CCP reactor with sensor flush-mounted in the substrate holder. (b) PET film substrate (marked in red) on top of the probe head. (c) Prototype of the spMRP; electrodes covered with ceramic layer.

known in advance, a correction factor is conceivable to account for these issues in the model. Considering an industrial deposition process with typical materials as in Table II and regular coating thicknesses, the applicability of the proposed concept as well as its insensitivity to additional dielectric layers can be expected without limitations. Remarkably, materials with higher relative permittivities appear to have lower influence on the resonance parameters even at very high coating thicknesses and if high losses are present.

V. Measurements

To validate the proposed concept, measurements in a magnetron CCP reactor [41] during a sputter deposition, according to the schematic in Fig. 2, are performed. Photographs of the real measurement setup can be seen in Fig. 8. The driven electrode of the reactor is operated at 13.56 MHz and supplied with an input power of P_{in}, which is adjusted to the respective plasma-dependent admittance using a tunable automatic matching network. The final electron density n_{e} in the plasma is mainly linked to P_{in}. The collision frequency ν, on the other hand, is mainly dependent on the gas pressure p_{gas}. Yet, there is generally a correlation between all external and internal parameters. For example, a change in p_{gas} also affects n_{e}. Thus, n_{e} and ν are coupled together in a real process. Depending on the actual conditions during the process, the effect of this coupling is pronounced to a greater or lesser extent.

As in the simulations, a PET film substrate with a thickness of 100 µm is used. Aluminum is applied as a target material. Together with the process gases that are argon and oxygen at the gas flow rates of 20 and 5 sccm, respectively, a deposition of Al_2O_3 on the PET film can be achieved. The spMRP prototype is flush-mounted in the holder right behind the substrate, on its plasma-remote side, and is connected to a Rohde & Schwarz ZVL6 VNA via vacuum feedthrough. In order to minimize a possible gap between the probe head and the substrate, the PET film is adhered to the cylinder topside. However, mechanical fixation might be a preferred solution in future setups. For the measurements, the complex reflection factor $\underline{S}_{11}$ is measured in a frequency range between 100 MHz and 2 GHz. All plasma measurements are vacuum compensated by subtracting a measurement of the evacuated reactor without plasma. Subsequently, the admittance $\underline{Y}$ is calculated [see 11]. As in the simulations, the resonance parameters are extracted from the normalized real part of $\underline{Y}$. Once the plasma state is reached, the deposition process starts and is maintained as long as the plasma itself remains excited. Thus, with ongoing process duration, the Al_2O_3 layer thickness inevitably increases on the PET film. The process is monitored for approximately 23 min with a measurement taken every 2 s.

Fig. 9 shows the evaluated f_{res} and Δf for this time window, which are displayed together with the externally supervised input power P_{in} and gas pressure p_{gas}. Here, the color of the respective graph corresponds to the color of the associated ordinate axis. In the plot, six zones, labeled A–F, are highlighted to simplify the referencing in the following discussion. Beginning with zone A, the monitoring has already started before all external requirements have been reached and prior to the actual plasma excitation. As discussed in Section II, a resonance is not present without a plasma. Thus, a random maximum is tracked in the measured data leading to random fluctuations of the monitored f_{res} in this zone. The same is valid for the parameter Δf, which shows a very small randomly varying width without any further significance. As soon as the plasma is excited (at $P_{\mathrm{in}} = 40$ W and $p_{\mathrm{gas}} \approx 3$ Pa), marked in Fig. 9 as Plasma: on, both resonance parameters stabilize basically immediately at certain values. While f_{res} settles at 0.34 GHz, Δf reaches a maximum of 156 MHz. After that, the external process parameters are kept constant at their respective values for around 10 min (see zone B). As can be seen, f_{res} remains exceptionally stable during that time being parallel to the curve of P_{in}. On the other hand, the curve of Δf initially exhibits an exponential drift behavior, which flattens rapidly over time, so that it runs almost parallel to the curve of p_{gas}. Between minute two and eleven, however, a minor drift of about -0.44 MHz/min remains. Since the trend is negative, this behavior cannot be explained due to coating material losses (e.g., compare Fig. 7). In case of a temperature-related drift of the VNA, f_{res} would shift as well. Thus, a real temporal drift of the plasma's collision frequency ν can be observed here, highlighting the importance of plasma monitoring based on internal parameters. In zone C, P_{in} is changed to 130 W for 20 s before being reset to the previous value of 40 W. As can be seen, f_{res} follows immediately the changes of P_{in}. At the same time, these massive power variations lead to instabilities in the plasma as revealed by fluctuations of Δf. At around 12 min, the input power is shortly reduced to 10 W before it is set to 20 W. As a consequence of the initial low value for P_{in}, the plasma destabilizes, thus resulting in a notable flickering of its emitted light. Therefore, the evaluated f_{res} also fluctuates accordingly between 0.25 and 0.3 GHz,

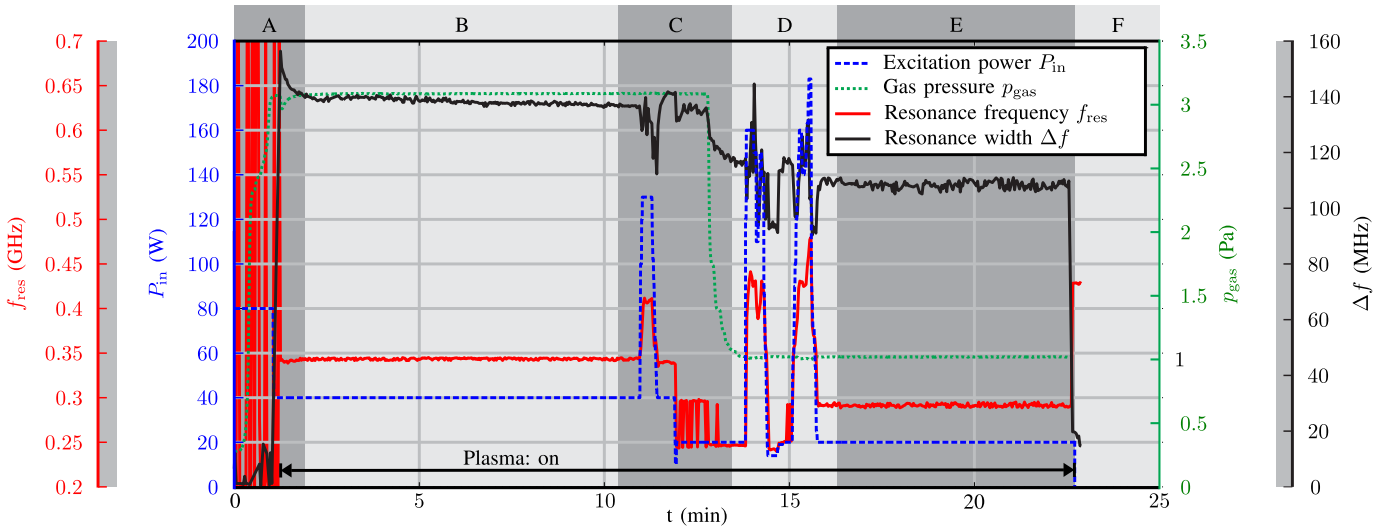

Fig. 9. Monitoring results with the spMRP in a magnetron CCP during dielectric deposition of Al_2O_3 on a PET film substrate (process gases: 20 sccm Ar + 5 sccm O_2). Recorded external parameters P_{in} (blue dashed line) and p_{gas} (green dotted line) together with the evaluated resonance parameters f_{res} (red solid line) and Δf (black solid line).

confirming the already visible instability. During this period, p_{gas} is reduced to approximately 1 Pa resulting, as seen before, in an exponential drift of Δf. Subsequently, P_{in} is significantly varied as indicated by the two high peaks in zone D. Once more, f_{res} follows immediately these rapid changes, which also affects Δf resulting in its strong fluctuations. In zone E, P_{in} and p_{gas} are kept constant again for around more 7 min at a low power of 20 W and 1 Pa, respectively. Consequently, both resonance parameters stabilize at $f_{res} \approx 0.3$ GHz and $\Delta f \approx 108$ MHz, thus resulting in parallel curves. Unlike in zone B, a drifting behavior of Δf cannot be observed. Finally, the plasma excitation is terminated and the monitoring is stopped (see zone F).

The presented monitoring results during a sputter deposition with Al_2O_3 on a PET film substrate confirm the applicability of the concept and its practical insensitivity to additional dielectric coatings. Therefore, deviations of the plasma can be supervised in real time and, if necessary, a quick process adjustment can be performed. At the same time, the probe had basically no influence on the plasma due to its minimally invasive design as well as arrangement behind the substrate to be coated.

VI. Conclusion

In this article, we have presented a minimally invasive concept for supervision and control of plasma-assisted dielectric deposition processes, which is based on the pMRP. Mounted on the plasma-remote side of a dielectric substrate to be coated, the configuration allows a penetration of the sensor's electric field through all intermediate dielectric layers into the plasma. Thus, a perturbation-free monitoring of important process-relevant plasma parameters, such as electron density and collision frequency, via resonance frequency and width is enabled. Compared to our previous work in [27], an expanded and more detailed description of the monitoring concept as well as an extensively enlarged simulative investigation in CST Microwave Studio considering a broad range of coating materials and thicknesses as well as an additional evaluation of the resonance width have been presented. Considering coating thicknesses up to 100 µm and relative permittivities higher than 2, a worst case deviation of the resonance frequency below 2.5% and of the width below 8% with respect to the coating-free case could be observed in the simulations. Hence, the concept was able to demonstrate its insensitivity to additional dielectric coatings in several pseudo-deposition processes. To validate its performance in practice, real-time plasma monitoring on the backside of a PET film substrate during a sputter deposition with Al_2O_3 was performed and the results were compared with parallel supervised external process parameters. The results confirm the suitability of the proposed approach in the demanding environment of dielectric deposition processes, in which alternative systems might not be applicable. Other existing concepts, such as Langmuir probes, optical emission spectroscopy, or other APRS probes, might be invasive, depend upon a complex model of a specific plasma, require a difficult interpretation of ambiguous data, or are negatively affected by the deposited material. Although higher material conductivities complicate a penetration of the sensor's fields into the plasma, long-term monitoring is also conceivable in case of semiconductor depositions. First estimates of the wave penetration depth in typical semiconductor materials (e.g., silicon) show that in the operating frequency range of the sensor, an interaction with the plasma can still take place. Here, a worst case penetration depth larger 50 µm for a conductivity of 10^3 S/cm, a relative permittivity of 12, and a maximum frequency of 1 GHz can be estimated. Thus, the proposed monitoring concept can make a significant contribution to improving quality and yield of industrial thin-film processes.

References

[1] M. Ohring, *Materials Science of Thin Films*, 2nd ed. Boston, MA, USA: Academic, 2001.
[2] T. Schneller *et al.*, *Chem. Solution Deposition Funct. Oxide Thin Films*, Vienna, Austria: Springer, 2013.

[3] L. A. Dobrzański, K. Lukaszkowicz, A. Zarychta, and L. Cunha, "Corrosion resistance of multilayer coatings deposited by PVD techniques onto the brass substrate," *J. Mater. Process. Technol.*, vols. 164–165, pp. 816–821, May 2005.

[4] A. Baptista, F. Silva, J. Porteiro, J. Míguez, and G. Pinto, "Sputtering physical vapour deposition (PVD) coatings: A critical review on process improvement and market trend demands," *Coatings*, vol. 8, no. 11, p. 402, Nov. 2018.

[5] P. Frigeri, L. Seravalli, G. Trevisi, and S. Franchi, "Molecular beam epitaxy: An overview," *Comprehensive Semicond. Sci. Technol.*, vol. 3, pp. 480–522, 2011.

[6] R. L. Puurunen, "Surface chemistry of atomic layer deposition: A case study for the trimethylaluminum/water process," *J. Appl. Phys.*, vol. 97, no. 12, Jun. 2005, Art. no. 121301.

[7] H. Adachi, T. Hata, and K. Wasa, "5-Basic process of sputtering deposition," in *Handbook of Sputtering Technology*, K. Wasa, I. Kanno, and H. Kotera, Eds. Amsterdam, The Netherlands: Elsevier, 2012.

[8] M. Šimek, M. Cernák, O. Kylián, R. Foest, D. Hegemann, and R. Martini, "White paper on the future of plasma science for optics and glass," *Plasma Processes Polym.*, vol. 16, no. 1, Aug. 2018, Art. no. 1700250.

[9] M. Deilmann, S. Theiss, and P. Awakowicz, "Pulsed microwave plasma polymerization of silicon oxide films: Application of efficient permeation barriers on polyethylene terephthalate," *Surf. Coatings Technol.*, vol. 202, no. 10, pp. 1911–1917, 2008.

[10] L. Martinu and D. Poitras, "Plasma deposition of optical films and coatings: A review," *J. Vac. Sci. Technol. A, Vac. Surf. Films*, vol. 18, pp. 2619–2645, Nov. 2000.

[11] S. Shahidi, M. Ghoranneviss, M. Ahmadi, and A. Rashidi, "Effect of plasma treatment on self-cleaning of textile fabric using titanium dioxide," *Micro Nano Lett.*, vol. 10, no. 8, pp. 408–413, Aug. 2015.

[12] K. Wasa, M. Kitabatake, and H. Adachi, *Thin Films Material Technology: Sputtering of Compound Materials*. Norwich, NY, USA: William Andrew, 2004.

[13] P. Chelvanathan *et al.*, "Effects of RF magnetron sputtering deposition process parameters on the properties of molybdenum thin films," *Thin Solid Films*, vol. 638, pp. 213–219, Sep. 2017.

[14] N. Kumari, P. S. Das, N. K. Joshi, and P. K. Barhai, "Correlations of plasma parameters and properties of magnetron sputtered TiN films," *Eur. Phys. J. Appl. Phys.*, vol. 59, no. 2, p. 20302, Sep. 2012.

[15] L. Escobar-Alarcón, A. Arrieta, E. Camps, S. Romero, M. Fernandez, and E. Haro-Poniatowski, "Influence of the plasma parameters on the properties of aluminum oxide thin films deposited by laser ablation," *Appl. Phys. A, Solids Surf.*, vol. 93, no. 3, pp. 605–609, Jun. 2008.

[16] J. G. Quiñones-Galván *et al.*, "Influence of plasma parameters and substrate temperature on the structural and optical properties of CdTe thin films deposited on glass by laser ablation," *J. Appl. Phys.*, vol. 118, no. 12, Sep. 2015, Art. no. 125304.

[17] I. J. Kim and I. Yun, "Real-time plasma monitoring technique using incident-angle-dependent optical emission spectroscopy for computer-integrated manufacturing," *Robot. Comput.-Integr. Manuf.*, vol. 52, pp. 17–23, Aug. 2018.

[18] D. Pohle, C. Schulz, M. Oberberg, P. Awakowicz, and I. Rolfes, "Monitoring of industrial plasma processes using the multipole resonance probe," in *Proc. Eur. Microw. Conf. Central Eur. (EuMCE)*, Prague, Czech Republic, May 2019, pp. 604–607.

[19] M. B. Hopkins and J. F. Lawler, "Plasma diagnostics in industry," *Plasma Phys. Controlled Fusion*, vol. 42, no. 12B, pp. B189–B197, Dec. 2000.

[20] P. Laha *et al.*, "Development of RF plasma sputtered Al_2O_3–TiO_2 multilayer broad band antireflecting coatings and its correlation with plasma parameters," *Appl. Surf. Sci.*, vol. 258, no. 7, pp. 2275–2282, 2012.

[21] C. Schulz *et al.*, "The multipole resonance probe: Evolution of a plasma sensor," in *Proc. IEEE Sensors*, Baltimore, MD, USA, Nov. 2013, pp. 1–4.

[22] C. Schulz, T. Styrnoll, P. Awakowicz, and I. Rolfes, "The planar multipole resonance probe: Challenges and prospects of a planar plasma sensor," *IEEE Trans. Instrum. Meas.*, vol. 64, no. 4, pp. 857–864, Apr. 2015.

[23] M. Lapke, T. Mussenbrock, and R. P. Brinkmann, "The multipole resonance probe: A concept for simultaneous determination of plasma density, electron temperature, and collision rate in low-pressure plasmas," *Appl. Phys. Lett.*, vol. 93, no. 5, Aug. 2008, Art. no. 051502.

[24] D. Pohle *et al.*, "Progression of the multipole resonance probe: Advanced plasma sensors based on LTCC-technology," in *Proc. 48th Eur. Microw. Conf. (EuMC)*, Madrid, Spain, Sep. 2018, pp. 239–242.

[25] D. Pohle *et al.*, "A stacked planar sensor concept for minimally invasive plasma monitoring," in *Proc. Asia–Pacific Microw. Conf. (APMC)*, Kyoto, Japan, Nov. 2018, pp. 1315–1317.

[26] M. Friedrichs and J. Oberrath, "The planar multipole resonance probe: A functional analytic approach," *EPJ Techn. Instrum.*, vol. 5, no. 1, p. 7, Aug. 2018.

[27] D. Pohle, C. Schulz, M. Oberberg, P. Awakowicz, and I. Rolfes, "Minimally invasive supervision of plasma-assisted dielectric deposition processes," in *IEEE MTT-S Int. Microw. Symp. Dig.*, Bochum, Germany, Jul. 2018, pp. 163–165.

[28] H. Conrads and M. Schmidt, "Plasma generation and plasma sources," *Plasma Sources Sci. Technol.*, vol. 9, no. 4, pp. 441–454, Oct. 2000.

[29] W. M. Manheimer, L. E. Sugiyama, and T. H. Stix, *Plasma Science and the Environment*. College Park, MD, USA: American Institute of Physics, 1996.

[30] J. A. Bittencourt, *Fundamentals of Plasma Physics*. New York, NY, USA: Springer, 2004.

[31] M. A. Lieberman and A. J. Lichtenberg, *Principles of Plasma Discharges and Materials Processing*. New York, NY, USA: Wiley, 2005.

[32] M. Lapke *et al.*, "The multipole resonance probe: Characterization of a prototype," *Plasma Sources Sci. Technol.*, vol. 20, no. 4, May 2011, Art. no. 042001.

[33] C. Schulz and I. Rolfes, "Effect of pseudo collisions on plasma diagnostics," in *Proc. IEEE SENSORS*, Glasgow, U.K., Oct. 2017, pp. 1–3.

[34] L. Tonks and I. Langmuir, "Oscillations in ionized gases," *Phys. Rev.*, vol. 33, no. 2, pp. 195–210, Feb. 1929.

[35] N. S. J. Braithwaite and R. N. Franklin, "Reflections on electrical probes," *Plasma Sources Sci. Technol.*, vol. 18, no. 1, Nov. 2008, Art. no. 014008.

[36] M. Lapke, J. Oberrath, T. Mussenbrock, and R. P. Brinkmann, "Active plasma resonance spectroscopy: A functional analytic description," *Plasma Sources Sci. Technol.*, vol. 22, no. 2, Nov. 2012, Art. no. 025005.

[37] C. Schulz, T. Styrnoll, R. Storch, P. Awakowicz, T. Musch, and I. Rolfes, "The multipole resonance probe: Progression and evaluation of a process compatible plasma sensor," *IEEE Sensors J.*, vol. 14, no. 10, pp. 3408–3417, Oct. 2014.

[38] D. Pohle *et al.*, "An advanced high-temperature stable multipole resonance probe for industry compatible plasma diagnostics," in *Proc. 11th German Microw. Conf. (GeMiC)*, Freiburg, Germany, Mar. 2018, pp. 235–238.

[39] C. Schulz *et al.*, "A novel radio-frequency plasma probe for monitoring systems in dielectric deposition processes," in *Proc. Int. Conf. Electromagn. Adv. Appl.*, Sep. 2012, pp. 728–731.

[40] M. Friedrichs, D. Pohle, I. Rolfes, and J. Oberrath, "Planar multipole resonance probe: Comparison of full-wave electromagnetic simulation and electrostatic approximation," in *Proc. Kleinheubach Conf.*, Miltenberg, Germany, Sep. 2019, pp. 1–3.

[41] M. Oberberg, J. Kallähn, P. Awakowicz, and J. Schulze, "Experimental investigations of the magnetic asymmetry effect in capacitively coupled radio frequency plasmas," *Plasma Sources Sci. Technol.*, vol. 27, no. 10, Oct. 2018, Art. no. 105018.

[42] J. Runkel, C. Schulz, I. Rolfes, M. Oberberg, and P. Awakowicz, "Monitoring of low pressure plasmas with a calibrated probe," in *Proc. German Microw. Conf. (GeMiC)*, Bochum, Germany, Mar. 2016, pp. 43–46.

[43] C. Schulz, *Novel Sensor Concepts for Plasma Diagnostics*, Munich, Germany: Verlag Dr. Hut, 2017.

[44] C. Schulz and I. Rolfes, "Plasma diagnostics in dielectric deposition processes," in *Proc. IEEE SENSORS*, Orlando, FL, USA, Oct. 2016, pp. 1–3.

[45] J. Robertson, "High dielectric constant oxides," *Eur. Phys. J. Appl. Phys.*, vol. 28, no. 3, pp. 265–291, Dec. 2004.

[46] T. Styrnoll, S. Bienholz, M. Lapke, and P. Awakowicz, "Study on electrostatic and electromagnetic probes operated in ceramic and metallic depositing plasmas," *Plasma Sources Sci. Technol.*, vol. 23, no. 2, Mar. 2014, Art. no. 025013.

[47] A. Salimian, R. Haghpanahan, A. Hasnath, and H. Upadhyaya, "Optical analysis of RF sputtering plasma through colour characterization," *Coatings*, vol. 9, no. 5, p. 315, May 2019.

Dennis Pohle (Graduate Student Member, IEEE) was born in Herne, Germany, in 1987. He received the B.Sc. and M.Sc. degrees in electrical engineering from Ruhr University Bochum, Bochum, Germany, in 2012 and 2014, respectively, where he is currently pursuing the Ph.D. degree in electrical engineering at the Institute of Microwave Systems.

Since 2014, he has been a Research Assistant with the Institute of Microwave Systems, Ruhr University Bochum. His current research interest includes plasma diagnostics, in particular the multipole resonance probe, radar signal processing, and 3-D electromagnetic field simulations.

Christian Schulz (Member, IEEE) received the Dipl.-Ing. and Dr.-Ing. degrees in electrical engineering from Ruhr University Bochum, Bochum, Germany, in 2009 and 2016, respectively.

From 2010 to 2016, he was a Research Assistant with the Institute of Microwave Systems, Ruhr University Bochum, where he has been a Post-Doctoral Researcher since 2016. His current fields of research are concerned with 3-D electromagnetic field simulations, plasma diagnostics, radar systems, and antenna design.

Dr. Schulz was a recipient of the IEEE Antennas and Propagation Society Doctoral Research Award in 2014 and the IEEE Microwave Theory and Techniques Society (IEEE MTT-S) Graduate Fellowship Award in 2015. In 2017, he received the Gert Massenberg Award for his doctoral thesis.

Moritz Oberberg was born in Essen, Germany, in 1990. He received the M.Sc. degree in electrical engineering from Ruhr University Bochum, Bochum, Germany, in 2014, where he is currently pursuing the Ph.D. degree in electrical engineering at the Institute of Microwave Systems.

Since 2014, he has been a Research Assistant with the Institute for Electrical Engineering and Plasma Technology, Ruhr University Bochum. His research interests include plasma deposition processes and plasma diagnostics, especially the multipole resonance probe, and its operation in industrial application for experimental characterization.

Peter Awakowicz received the Dipl.-Ing. degree in electrical engineering from RWTH Aachen, Aachen, Germany, in 1984, and the Dr.-Ing. degree in electrical engineering and the Habilitation degree in plasma technique from the Technical University of Munich (TU Munich), Munich, Germany, in 1990 and 1999, respectively.

In 1990, he became a Research Assistant at TU Munich. From 2000 to 2003, he was a Privatdozent in the research field of plasma technology at TU Munich. Since 2003, he has been leading the Institute for Electrical Engineering and Plasma Technology, Ruhr University Bochum, Bochum, Germany. He has been a Speaker of the Collaborative Research Center SFB-TR87 since 2010. His fields of research concern plasma technique, plasma diagnostics, and multifunctional surfaces.

Ilona Rolfes (Member, IEEE) received the Dipl.-Ing. and Dr.-Ing. degrees in electrical engineering from Ruhr University Bochum, Bochum, Germany, in 1997 and 2002, respectively.

From 1997 to 2005, she was with the High Frequency Measurements Research Group, Ruhr University Bochum, as a Research Assistant. From 2005 to 2009, she was a Junior Professor with the Department of Electrical Engineering, Leibniz University Hannover, Hannover, Germany, where she became the Head of the Institute of Radio frequency and Microwave Engineering in 2006. Since 2010, she has been leading the Institute of Microwave Systems, Ruhr University Bochum. Her fields of research concern high-frequency measurement methods for vector network analysis, material characterization, noise characterization of microwave devices, sensor principles for radar systems, and wireless solutions for communication systems.